ISBN: 978-3-95450-223-3 ISSN: 2673-7000 doi:10.18429/JACoW-NAPAC2019-TUYBB5

# DESIGN AND ANALYSIS OF A HALO-MEASUREMENT DIAGNOSTICS*

C. J. Marshall, P. Piot[1], Northern Illinois University, DeKalb, IL, USA
S. V. Benson, J. Gubeli,
Thomas Jefferson National Accelerator Laboratory, Newport News, VA, USA
J. Ruan, Fermi National Accelerator Laboratory, Batavia, IL, USA
[1]also at Fermi National Accelerator Laboratory

*Abstract*

A large dynamical-range diagnostics (LDRD) design at Jefferson Lab will be used at the (Fermilab Accelerator Science and Technology-Integrable Optics Test Accelerator) FAST-IOTA injector to measure the transverse distribution of halo associated with a high-charge electron beam. One important aspect of this work is to explore the halo distribution when the beam has significant angular momentum (i.e. is magnetized). The beam distribution is measured by recording radiation produced as the beam impinges a YAG:Ce screen. The optical radiation is split with a fraction directed to a charged-couple device (CCD) camera. The other part of the radiation is reflected by a digital micro-mirror device (DMD) that masks the core of the beam distribution. Combining the images recorded by the two cameras provides a measurement of the transverse distribution over a large dynamical range $O(10^5)$. The design and analysis of the optical system is discussed.

## INTRODUCTION

A beam halo is generally considered to be the low intensity of particles that surround the main core of the beam. Particle within the beam halo do not generally participate in the front-end application of the beam but can limit the overall performances of an accelerator. For instance, a particle in the beam halo can be lost and results in beamline-component radiological activation or damaged hardware. Particle loss could especially hinder the operation of high-average current electron accelerator such as needed for electron-beam cooling [1] in the foreseen Electron-Ion Collider (EIC). Therefore understanding the source of halo formation could help its mitigation which ultimately improves accelerator performances. Consequently developing a reliable halo-measurement beam diagnostics is critical.

Over the years, the beam halo distribution is often measured using a coronographic technique where a mask block the beam core and a charged-coupled device (CCD) detector measured the unlock distribution. Such a technique supported the exploration of halo formation in high-duty-cycle photoinjector [2]. Given the advances in micro-fabrication, the coronographic method was improved to use dynamical mask employing digital micro-mirror device (DMD) [3,4].

This paper discusses the implementation of a flexible halo diagnostics using a DMD similar to Ref. [4]. We detail the optical design of such a system and develop numerical simulation to explore its performances. Ultimately, the system will be tested on an electron-beam test accelerator and support the investigation of halo formation in magnetized electron beams such as required for magnetized electron cooling.

* This work is supported by the U.S. Department of Energy, Office of Science, Office of Nuclear Physics, under contracts DE-AC05-06OR23177 and DE-AC02-07CH11359.

## OVERVIEW

A diagram of the optical setup associated with the large-dynamical range diagnostics (LDRD) appears in Fig. 1. In brief, the optical radiation emitted as an electron beam impinges on a YAG:Ce screen is collected and imaged by a pair of lenses on the DMD surface which is further imaged on the CCD chip of the camera. The DMD (development kit from DLP model LightCrafter 6500 1080p) consists of an array of 1920 × 1080 mirrors and is set up so mask the central part of the beam before imaging on CCD#2. In our setup, a

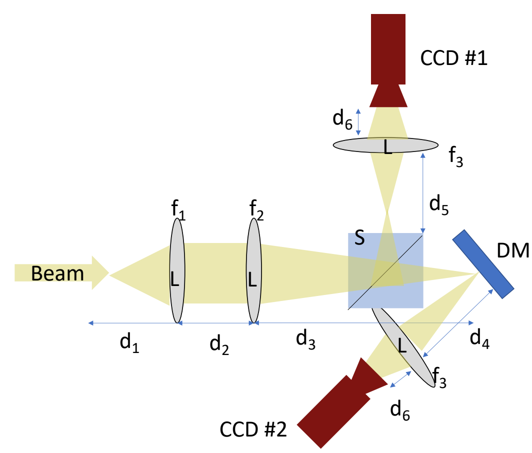


Figure 1: Diagram of the optical setup used in the LDRD. The labels “L”, “S” correspond to the locations of the lenses and splitter.

50-50 beam splitter is placed upstream of the DMD to direct half of the light to another CCD camera (CCD#1). This dual-CCD approach was first adopted in Ref. [5]. Images from both of these CCDs (operated with different gains) are simultaneously recorded and combined to reconstruct the beam profile.

## OPTICAL SYSTEM

We first consider the optical function of the setup shown in Fig. 1 and note that both arms of the diagnostics are identical. They can be represented by an unfolded configuration

Content from this work may be used under the terms of the CC BY 3.0 licence (© 2019). Any distribution of this work must maintain attribution to the author(s), title of the work, publisher, and DOI

ISBN: 978-3-95450-223-3 ISSN: 2673-7000 doi:10.18429/JACoW-NAPAC2019-TUYBB5

consisting of a source, and detector located on each side of a three-lens imaging system. The optical radiation emitted as the electron beam hits the YAG:Ce screen mirrors the electron-beam transverse distribution, therefore, imaging the radiation provides information on the electron-beam parameters. The optical system is required to image the YAG:Ce-screen surface on the DMD chip to enable the masking of the core. Likewise, the masked distribution (at the DMD surface) is imaged on the CCD chip.

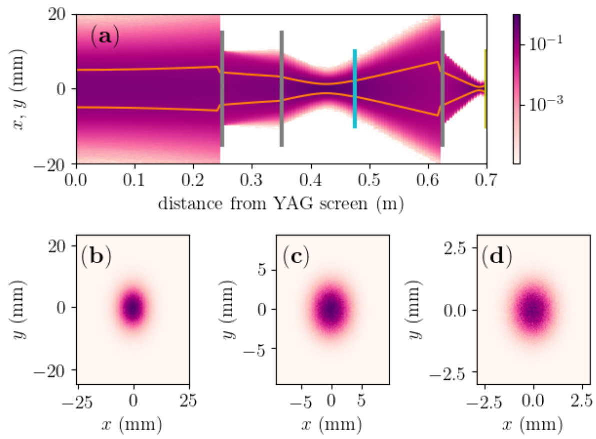


Figure 2: Peak-normalized beam intensity along the optical system [(a), logarithmic false-color map] and associated beam envelope [(a), orange trace]. Transverse beam distribution recorded at the locations of the source (b), DMD (c) and CCD camera (d). In plot (a) the grey, blue and green rectangles correspond to the locations of the lenses, DMD, and CCD chip. The beam propagates from the left to right with CCD array at 0.7 m.

As a first step, the system can be designed using the ABCD matrix formalism [6]. Assuming the system to be cylindrical symmetric and focusing on one of the transverse planes only, the mapping of a ray with coordinate $\mathbf{r}_0 \equiv (r_0, \theta_0)$, where $r_0$ and $\theta_0$ are the initial position and divergence associated to a given ray, is described by the transformation $\mathbf{r}_0 \to \mathbf{r} = R\mathbf{r}_0$ where $R$ is the 2×2 ABCD matrix. Given that $r = Ar_0 + B\theta_0$, the imaging imposes the conditions $B \equiv R_{12} = 0$ and other parameters can be selected to set the optical magnification $\mathcal{M}$ by setting $A \equiv R_{11} = \mathcal{M}$.

Table 1: Parameters Associated with the Object and Image Planes

| **element** | **field-of view/size** (mm×mm ) | **pixel size** (µm×µm) |
|---|---|---|
| YAG screen | 15 × 15 | – |
| DMD array | 8.16 × 14.52 | 7.6 × 7.6 |
| CCD array | 8.45 × 7.07 | 3.45 × 3.45 |

The overall magnification $\mathcal{M}$ between the YAG:Ce screen and CCD camera is given by the desired field of view and alignment tolerance. Likewise the magnification between the YAG:Ce and DMD $\mathcal{M}_1$ and between the DMD and CCD camera images $\mathcal{M}_2$ related to the size of the DMD and CCD arrays; see Table 1. The CCD parameters assumed correspond to the Prosilica GC 2450 CCD Camera equipped with a SONY ICX625 CCD sensor. As an example we consider a system providing the magnifications $\mathcal{M}_1 = \frac{1}{2}$ and $\mathcal{M}_2 = \frac{1}{2}$ corresponding to $\mathcal{M} = \mathcal{M}_1\mathcal{M}_2 = \frac{1}{4}$.

Table 2: Numerical Values of Optical Elements from YAG:Ce screen to DMD

| **optical element** | **positions** (mm) | **focal length** (mm) |
|---|---|---|
| YAG:Ce screen | 0 | – |
| lens L1 | 250 | 250 |
| lens L2 | 350 | 125 |
| DMD | 475 | – |
| lens L3 | 625 | 50 |
| CCD | 700 | – |

For the CCD array parameter listed in Table 1 one could in principle select $\mathcal{M}_2 \simeq 1$ and our choice is conservative to relax alignment tolerances. By fixing the to parameters $\mathcal{M}_1$ and $\mathcal{M}_2$, imposing the imaging conditions $B_1 = B_2 = 0$ (where the subscripts 1 and 2 refer respectively to the elements of the transfer matrix between the YAG and DMD and the DMD and CCD), we arrive to a system of equations relating the focal lengths and position of lenses. Constraining the location of the first lens to be at 250 mm from the source (due to the vacuum chamber and optical port distance), and imposing the system to fit on a $1' \times 2'$ optical breadboard results in a set of focal lengths and distances. The distances are tuned to ensure the obtained focal lengths correspond to off-the-shelve lenses; see Table 2. All lenses are considered to have a $1''$-diameter aperture.

To further quantify the performance of the optical system, a PYTHON ray-tracing program was developed. The program allows for several sources to be considered and model the beam as a collection of rays which are propagated via the ABCD formalism. The program is vectorized to allow for very fast calculations in the 4-dimensional coordinate system $(x, x', y, y')$. The system described in Table 2 was implemented assuming an input Gaussian light source with 5-mm rms size and 12.5-mrad rms divergence (corresponding to the parameter of the electron beam). Figure 4(a) shows the beam-envelope evolution along the optical system and the lower density plots correspond to light-intensity distribution at the source (b), DMD (c), and CCD (d). Further, replacing the source with a patterned source (consisting of five concentric circles) shows that an image of the source with proper magnification is formed on the DMD and CCD arrays; see Fig. 3.

Content from this work may be used under the terms of the CC BY 3.0 licence (© 2019). Any distribution of this work must maintain attribution to the author(s), title of the work, publisher, and DOI

ISBN: 978-3-95450-223-3 ISSN: 2673-7000 doi:10.18429/JACoW-NAPAC2019-TUYBB5

Content from this work may be used under the terms of the CC BY 3.0 licence (© 2019). Any distribution of this work must maintain attribution to the author(s), title of the work, publisher, and DOI

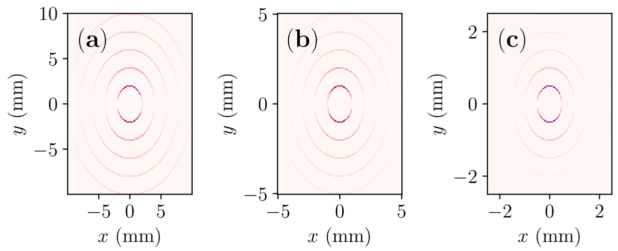


Figure 3: Patterned source (a) and corresponding images on the DMD (b) and CCD (c) arrays.

## CORE MASKING & BEAM RECONSTRUCTION

The PYTHON ray-tracing program was also used to explore the effect of the DMD. Figure 4 shows the beam envelope and associated images when the DMD is turned on. The DMD mask was simulated by the transformation $x'_0 \longrightarrow x' = x'_0 + \psi$ over a given area $\mathcal{A}$. Here $\psi$ the tilt angle associated with

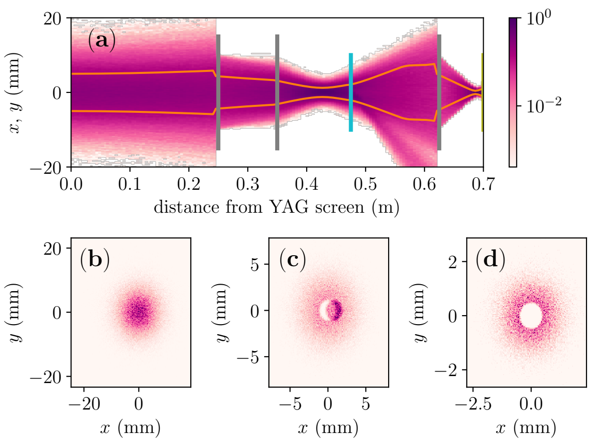


Figure 4: Same figure as Fig. 2 but with DMD turned on.

the micro-mirrors within the area $\mathcal{A}$. For the simulation presented in Fig. 4 we considered $\psi = 10°$ and set the area to be $\mathcal{A}$ to be the disk with radius $\rho = 1$ mm. The deflected beam corresponding to the core population is seen in Fig. 4(a) the title angle and distance between the DMD and lens L3 is selected to ensure the deflected population is outside the aperture of L3 resulting in the final image to have no light in its center; see Fig. 4(c).

It should be noted that for more complex beam distribution the area can be defined as a function of pixel intensity on the CCD so to apply the mirror tilt on all pixels with values above a given threshold. Such an algorithm can in principle be dynamically implemented. It should be noted that in our present investigation we consider the same tilt angle to be applied to all micro-mirrors other configurations, e.g. deflecting the beam radially, will be investigated experimentally.

A final step in measuring the beam over a large dynamical range (DR) is to combine the full-beam image with the

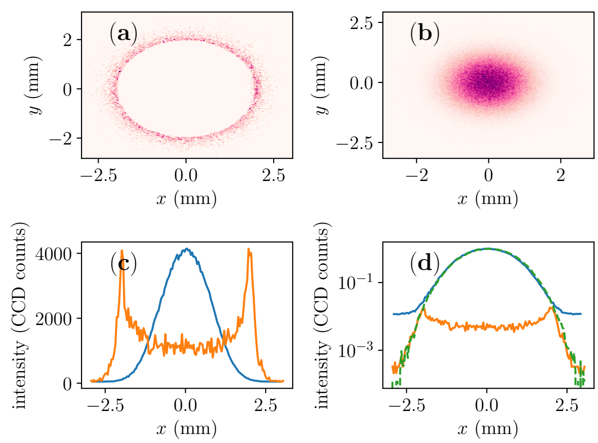


Figure 5: Example of beam reconstruction of a dynamical range of $10^4$. Simulated from CCD#2 (a) and #1 (b) with corresponding projection [respectively shown as orange and blue trace, (c)] and reconstructed profile (d).

masked-core image respectively recorded by CCD#1 and #2. Figure 5 present such simulations and demonstrate that a DR $\sim 10^4$ is achieved. For these calculations, the CCD camera were taken to have a 12-bit pixel depth and we assume that the lower 5 bits were unusable due to noise. Besides, noise fluctuations were added to each pixel. The gain of the two cameras was set so that the signals extend over the full DR of the CCD; see Fig. 5(c) yielding the reconstructed profile shown in Fig. 5(d). The achieved DR is obtained in a single shot and could be improved, albeit in a multishot mode, by taking several masked images for different masking patterns (e.g. by varying the threshold pixel value).

## FUTURE PLANS

We expect the developed optics to be tested in the next few weeks before installation on the FAST/IOTA electron accelerator [7] in support of a magnetized-beam generation experiment [8]. In an intermediary step, we are also considering possible tests of the diagnostics in the AWA facility [9] where high-charge magnetized beams were recently generated [10].

## REFERENCES

[1] S. V. Benson *et al.*, "Development of a Bunched Beam Electron Cooler Based on ERL and Circulator Ring Technology for the Jefferson Lab Electron-Ion Collider", in *Proc. 11th Workshop on Beam Cooling and Related Topics (COOL'17)*, Bonn, Germany, Sep. 2017, pp. 72–76. doi:10.18429/JACoW-COOL2017-WEM12

[2] G. Haouat *et al.*, "Experimental study of the ELSA electron-beam halo," *AIP Conf. Proc.*, vol. 333, p. 245, 1995.

[3] J. Egberts, C. P. Welsch, "Flexible core masking technique for beam halo measurements with high dynamic range," *J. Instrum. (JINST)*, vol. 5, p. P040105, 2010. doi:10.1088/1748-0221/5/06/P06007

ISBN: 978-3-95450-223-3 ISSN: 2673-7000 doi:10.18429/JACoW-NAPAC2019-TUYBB5

[4] H. D. Zhang *et al.,* "Beam halo imaging with a digital optical mask," *Phys. Rev. ST Accel. Beams,* vol. 15, p. 072803, 2012. doi:10.1103/PhysRevSTAB.15.072803

[5] P. E. Evtushenko, "Large Dynamic Range Beam Diagnostics for High Average Current Electron LINACs", in *Proc. 5th Int. Particle Accelerator Conf. (IPAC'14)*, Dresden, Germany, Jun. 2014, pp. 1900–1905. doi:10.18429/JACoW-IPAC2014-WEYB01

[6] J. Peatross and M. Ware, *Physics of Light and Optics*, 2015 edition, https://optics.byu.edu/BYUOpticsBook_2015.pdf

[7] FAST, https://fast.fnal.gov

[8] A. T. Fetterman, J. Ruan, P. Piot, S. V. Benson, F. E. Hannon, and S. Wang, "Generation of High-Charge Magnetized Electron Beams Consistent With JLEIC Electron Cooling Requirement", presented at the North American Particle Accelerator Conf. (NAPAC'19), Lansing, MI, USA, Sep. 2019, paper TUPLM20.

[9] AWA, https://www.anl.gov/awa

[10] T. Xu *et al.*, "Generation High-Charge of Flat Beams at the Argonne Wakefield Accelerator", in *Proc. 10th Int. Particle Accelerator Conf. (IPAC'19)*, Melbourne, Australia, May 2019, pp. 3337–3340. doi:10.18429/JACoW-IPAC2019-WEPTS094

Content from this work may be used under the terms of the CC BY 3.0 licence (© 2019). Any distribution of this work must maintain attribution to the author(s), title of the work, publisher, and DOI